



Tumor Microenvironment Stimuli-Responsive Polymeric Prodrug Micelles for Improved Cancer Therapy

Zhiqiang Zhang¹ · Miao Yu¹ · Tong An¹ · Jun Yang¹ · Meijuan Zou¹ · Yinglei Zhai² · Wei Sun² · Gang Cheng¹

Received: 28 June 2019 / Accepted: 28 September 2019 / Published online: 10 December 2019
© Springer Science+Business Media, LLC, part of Springer Nature 2019

ABSTRACT

Purpose The discovery of nano drug delivery system has rendered a great hope for improving cancer therapy. However, there are some inevitable obstacles that constrain its development, such as the physical and biological barriers, the toxicity of carrier materials and the physiological toxicity of drugs. Here, we report a polymeric prodrug micelle (PPM) with pH/redox dual-sensitivity, which was prepared using methoxy poly (ethylene glycol) (mPEG) with favorable biosafety to improve cancer therapy.

Method The tumor microenvironment stimuli-responsive PPMs were prepared and characterized *in vitro* and *in vivo*.

Results Our data displayed that the PPMs with excellent biocompatibility exhibited the stimuli-responsive drug release behavior under the microenvironment of cancer cells, superior cellular internalization and lower cytotoxicity. A new method to control drug release behavior was proposed by comparing the release behavior of PPMs formed by PEG of different molecular weight. Furthermore, the fabricated PPMs exhibited the “oral-like” blood concentration curve, improved biodistribution, reduced tissue toxicity and excellent antitumor efficiency *in vivo*. Consistently, these results indicated that

PPMs improved chemotherapeutic efficiency and reduced side effects of the model drug doxorubicin (DOX).

Conclusion The prepared pH/redox dual-sensitive PPM enhanced the chemotherapy effect on the tumor site while reducing the physiological toxicity of DOX.

KEY WORDS controlled release · micelles · pH/redox dual-sensitive · polymeric prodrug · stimuli-responsive

ABBREVIATIONS

¹ H-NMR	Nuclear magnetic resonance
4-NPC	4-nitrophenyl chloroformate
4-CBA	4-Carboxybenzaldehyde
AUC	Area-under the curve
CCK-8	Cell proliferation and toxicity test kit cell counting kit-8
CE	Cellulose ester
CLSM	Confocal laser scanning microscope
DCM	Dichloromethane
DDS	Drug delivery system
DiR	1,1-dioctadecyl-3,3,3,3-tetramethylindotricarbocyanine iodide
DLC	Drug loading content
DLS	Dynamic light scattering
DMAP	4-Dimethylaminepyridine
DMSO	Dimethyl sulfoxide
DNR·HCl	Daunorubicin hydrochloride
DOX·HCl	Doxorubicin hydrochloride
EDC·HCl	N-(3-Dimethylaminopropyl)-N'-ethylcarbodiimide hydrochloride
EPR	Enhanced permeability and retention
FDA	United States Food and Drug Administration
FT-IR	Fourier transform infrared
GSH	Glutathione
HPLC	High performance liquid chromatography
H&E	Hematoxylin and eosin

Electronic supplementary material The online version of this article (<https://doi.org/10.1007/s11095-019-2709-1>) contains supplementary material, which is available to authorized users.

✉ Wei Sun
sunwei19801208@163.com

✉ Gang Cheng
chenggang63@hotmail.com

¹ Department of Pharmaceutics, School of Pharmacy
Shenyang Pharmaceutical University
Shenyang 110016, People's Republic of China

² Department of Biomedical Engineering, School of Medical Device
Shenyang Pharmaceutical University
Shenyang 110016, People's Republic of China

MDR	Multi-drug resistance
PBS	Phosphate buffer solution
PEG	Poly (ethylene glycol)
PPM	Polymeric prodrug micelle
RES	Reticuloendothelial system
ROS	Reactive oxygen species
SEM	Scanning electron microscope
SD	Sprague-Dawley
SPSS	Statistic package for social science
TEA	Triethylamine
TEM	Transmission electron microscopy
THF	Tetrahydrofuran

INTRODUCTION

Many drug delivery systems (DDSs) designed for anti-tumor drugs, which has shown many benefits including high cargo loading, controlled drug release and enhanced tumor-selective targeting capability, *etc.* (1,2). However, the clinical application of many materials employed in DDSs is restrained due to their inevitable toxicity (3–6). Taking the nanoparticles act as a case in point, the nanoparticles may cause high level of damage to normal tissues and organs due to containing gold or mesoporous silica components, tissue accumulation and severe hemolysis are two abundant outcomes (7–9). The poly (amidoamine) dendrimers which has displayed prominently in drug delivery are limited for wide-spread clinical application because it is toxic to the cell membrane (10,11). Hence, the rational design of DDS by using materials without potential biosafety danger is critical in improving the chemotherapy effect on the tumor.

Recently, PEG has become the focus of new drug-loaded material and plays a crucial role in the field of DDSs because it exhibits advantageous properties in comparison with other materials, such as hydrophilicity, biocompatibility, biodegradability, and long-term circulation *in vivo* (12,13). PEG has been approved by the United States Food and Drug Administration (FDA) for clinical applications of humans. Previous researches have shown that nanomaterials modified by PEG showed improved stability and reduced side effects (14,15). Accordingly, PEG is usually employed as the hydrophilic block of nano-carriers of which the diameter can be controlled below 200 nm to accomplish the passive accumulation in tumor tissues via enhanced permeability and retention (EPR) effect (16–19).

PPMs have the advantages of loading drugs into polymer efficiently (20), improving drug stability (21) and controlling drug release (22) of prodrug, making it increasingly investigated for cancer therapy. Polymeric micelles as one of the most widely used DDSs can not only load drugs efficiently, but improve the pharmacokinetic and pharmacodynamics behavior of drugs (12,23–25). Prodrug polymers endow DDSs an

option to improve drug loading efficiency, increase water solubility of hydrophobic drugs and control physical form of DDSs (liquid preparation, semisolid preparation, *etc.*) (22,26). PPM systems have great benefits in avoiding the undesired drug leakage and premature drug release from polymer micelles, because of the covalent conjugation between polymers and antitumor drugs (27,28). Meanwhile, the “invisibility effect” of PEG can protect PPMs fabricated from PEG from recognizing by the reticuloendothelial system (RES) so that it can achieve long-term circulation (29). Altogether, PEG-containing PPMs are able to improve the stability via sparing from being rapidly metabolized or excreted by the body.

Although the long-term circulation of PEGylated PPMs dramatically prolongs the half-life time of drugs, it is critical for chemotherapeutics to fulfill the targeted release in tumor tissues (30–32). Fortunately, many studies have reported that polymeric prodrug can achieve rapid drug release through chemical bonds such as pH-responsive bonds (hydrazide, hydrazone and imine) (4,33), redox-responsive bonds (disulfide) (19) and reactive oxygen species (ROS) responsive bonds (thioether) (34). The tumor acidic microenvironment which pH even decreases to 5.0 is caused by the hypoxia and glycolysis of tumor cells (33). The high concentration of glutathione (GSH) inside tumor cells allows them to maintain an intense reducing circumstance (34). All these properties of tumor microenvironment allow DDSs containing cleavable chemical bonds to accelerate drug release at tumor sites or/and in tumor cells. The PPM systems can introduce the above sensitive chemical bonds to achieve rapid and targeted drug release at tumor tissues.

In order to avoid the undesired potential safety hazard caused by the complexity of multiple materials, we constructed a self-assembled PPM using the biocompatible polymer PEG (molecular weight of 2 K/5 K) and the model drug DOX. The PPM displayed prominent physiological stability, rapid drug release at tumor sites and reduced insecurity caused by excessive polymer material. The PEG shell helps the PPMs to achieve long-term circulation in the body. The tumor sites can be targeted by PPMs when PPMs has in the appropriate particle size. The stimuli-responsiveness (pH and redox sensitivity) of PPMs enables the rapidly release of DOX from the PPMs to the tumor cells rapidly and reduces side effects via maintaining stable of the micelles in physiological tissues. The morphology and size distribution of PPMs were characterized. Subsequently, the behaviors of *in vitro* drug release at pH 5.0 and 7.4 were investigated with and without the presence of GSH. The endocytosis ability and cytotoxicity of PPMs towards A549 cells were investigated by the cellular uptake and cell proliferation assays. In addition, a series of animal experiments were performed to further confirm the biodistribution and antitumor efficacy of PPMs.

MATERIALS AND METHODS

Materials

mPEG with the average M_n of 2 K and 5 K and N-(3-Dimethylaminopropyl)-N'-ethylcarbodiimide hydrochloride (EDC·HCl, 99.0%) were bought from Sigma-Aldrich and used according to the manufacturer's instruction. Doxorubicin hydrochloride (DOX·HCl), 1,1-dioctadecyl-3,3,3,3-tetramethylindotricarbocyanine iodide (DiR) and cellulose ester (CE) dialysis tubing (MWCO = 1000 Da) were purchased from Dalian Meilun Biotechnology Co., LTD. Bis(2-hydroxyethyl) disulfide (96.0%) was obtained from Alfa Aesar Chemical Co., Ltd. Pyridine (99.5%), triethylamine (TEA, 99.5%) and 4-nitrophenyl chloroformate (4-NPC, 97.0%) were purchased from J&K Scientific Co., Ltd. GSH, 4-Dimethylaminopyridine (DMAP, 99.0%), 4-Carboxybenzaldehyde (4-CBA, 98.0%) and all other reagents (analytical grade) were received from Aladdin Reagent Co., Ltd. and used without any further purification.

Cell proliferation and toxicity assay were performed to assess the toxicity of the drug by using Cell Counting Kit-8 (CCK-8) kit, which was purchased from Dalian Meilun Biotechnology Co., LTD. Human lung cancer cell line (A549) was a gift from School of Life Sciences and Biopharmaceuticals of Shenyang Pharmaceutical University and grown in DMEM medium containing 10% FBS in a 37°C incubator with 5% CO₂.

Instruments

The structures of synthesized materials were characterized by nuclear magnetic resonance (¹H-NMR) spectra (BRUKER 600 UltraShield™) and Fourier transform infrared (FT-IR) spectroscopy (BRUKER VERTEX 70 V). The morphology and particle size of the PPMs were investigated by transmission electron microscopy (TEM, Hitachi HT7700-SS), scanning electron microscope (SEM, Hitachi S-3400 N) and dynamic light scattering (DLS) assays (Malvern Zetasizer Nano S90). The specific surface area and relaxation time (spin-spin relaxation time, T₂) of the PPMs were determined by employing a particle surface property analyzer (Xigo Acorn Area), using low frequency pulsed NMR. The drug loading content and pharmacokinetics of the polymeric prodrugs were measured on a high performance liquid chromatography (HPLC) equipped with a Shimadzu LC-10ATVP Separations Module combined with SPD-10AVP variable-wavelength detector. The release of drug was examined using UV-vis instrument (Unico 2000 UV-vis). The cellular uptake was investigated with a Confocal Laser Scanning Microscope (CLSM, Zeiss LSM710). The cytotoxicity of PPMs was determined by a microplate reader (Multiskan™ FC). The tissue distribution study was detected using a Spectra Max M3

multi-function plate reader (Molecular Devices). The *in vivo* imaging test was performed on an IVIS Lumina III (PerkinElmer) small animal living imaging system.

Animals

Sprague-Dawley (SD) rats and BALB/c mice were obtained from Experimental Animal Center of Shenyang Pharmaceutical University. All animal experiments were conducted under the approval of the ethics committee of Shenyang Pharmaceutical University, Shenyang, China.

Synthesis of Disulfide Modified PEG (PEG-SS-OH)

4-nitrophenyl chloroformate functionalized mPEG_{2K} (PEG-NPC) was synthesized as reported previously (35). Briefly, catalytic amount of pyridine was added dropwise to the solution of PEG_{2K} (3 g, 1.5 mM) in dichloromethane (DCM) with continuous stirring. Subsequently, the 4-NPC (454 mg, 2.25 mM) solution in DCM was added slowly into the above mixture at 0°C. The reaction was placed at room temperature overnight under nitrogen protection. The solvent was removed under reduced pressure and the resultant was purified by precipitation in cold diethyl ether. The purification was performed at least in triplicate to collect PEG_{2K}-NPC. Yield: 89.2%, conversion ratio: 100.0%. All the conversion rate was calculated from the ¹H-NMR spectrum based on the ratio of proton peaks of the aromatic zone to the PEG peak of the fat zone. The corresponding calculation method will be presented in the "Results and Discussion" section. PEG_{5K}-NPC was prepared by the same method.

The introduction of the disulfide bond was easily achieved via a simple transesterification. Typically, catalytic amount of DMAP was added to the DCM solution of PEG_{2K}-NPC (1.5 g, 0.69 mM) and Bis(2-hydroxyethyl) disulfide (107 mg, 0.69 mM). The mixture was stirred vigorously under a nitrogen atmosphere at room temperature for 8 h. The solvent was removed under reduced pressure and the resultant product was dissolved by dimethyl sulfoxide (DMSO). Then the reaction solution was dialyzed against DMSO for 1 day and dialyzed against water for another day to obtain the purified PEG_{2K}-SS-OH. The resulting PEG_{2K}-SS-OH was collected by freeze-drying. Yield: 82.4%, conversion ratio: 93.2%. PEG_{5K}-SS-OH was synthesized via the same procedure.

Synthesis of Disulfide and 4-CBA Functionalized PEG (PEG-SS-CBA)

PEG-SS-CBA was synthesized via esterification. Typically, a solution of EDC·HCl (17.6 mg, 0.46 mM), DMAP (catalytic amount) and PEG_{2K}-SS-OH (1.0 g, 0.46 mM) was added to the solution of 4-CBA (83.0 mg, 0.55 mM) in DCM with magnetic stirring. Then the mixture was refluxed for another

8 h. After evaporation, the residue was redissolved in DCM (10 mL) and precipitated in freezing-cold. The process of precipitation was repeated at least twice to obtain pure PEG_{2K}-SS-CBA. Yield: 90.1%, conversion ratio: 88.4%. PEG_{5K}-SS-CBA was obtained via the same procedure.

Synthesis of pH and Redox Dual-Sensitive Polymeric Prodrug (PEG-SS-CBA-DOX)

Dual-sensitive polymeric prodrug PEG-SS-CBA-DOX was prepared via Schiff base reaction. In a typical example, the solution of PEG_{2K}-SS-CBA (600 mg, 0.257 mM) in DMSO was added dropwise to the solution of TEA (excessive amount) and DOX·HCl (108 mg, 0.257 mM) in DMSO. The reaction mixture was stirred in darkness (to prevent photolysis of DOX) at room temperature for 24 h. The resulting red powder PEG_{2K}-SS-CBA-DOX was obtained by dialysis against distilled water and lyophilization. PEG_{5K}-SS-CBA-DOX was prepared according to the same method. Yield: 95.6%, conversion ratio: 82.6%.

Synthesis of pH-Sensitive Polymeric Prodrug (PEG-CBA-DOX)

The esterification was utilized to accomplish the linkage between PEG and 4-CBA. 4-CBA (338 mg, 2.25 mM), EDC·HCl (431 mg, 2.25 mM) and DMAP (catalytic amount) were sequentially dissolved in 8 mL toluene and stirred at room temperature for 30 min. The solution of PEG_{2K} (3 g, 1.5 mM) in toluene was then added into the above mixture.

The reaction was allowed to proceed under nitrogen protection at 120°C for another 5 h. The product PEG_{2K}-CBA was purified by precipitation in cold diethyl ether and filtration. Yield: 87.3%, conversion ratio: 100.0%.

The solution of PEG_{2K}-CBA (1.0 g, 0.469 mM) in DMSO was added dropwise to the mixture containing DOX·HCl (272 mg, 0.469 mM) and TEA (475 mL, 0.469 mM). The reaction was kept in darkness (to prevent DOX photolysis) at room temperature with vigorous stirring for 24 h. The red powder PEG_{2K}-CBA-DOX was isolated and purified after dialysis and lyophilization. PEG_{5K}-CBA-DOX was prepared by the same method. Yield: 94.5%, conversion ratio: 96.8%.

Preparation and Characterization of PPMs

The PPMs were prepared by a self-assembling solvent evaporation method. Briefly, a 5 mL tetrahydrofuran (THF) solution of PEG-SS-CBA-DOX/PEG-CBA-DOX (50 mg) prodrug was added dropwise into deionized water (50 mL) and continued stirring at ambient temperature for 24 h. After passing through a 0.22 μm microfiltration membrane, the collected aqueous solution was lyophilized to obtain the PPMs.

To determine the drug loading content (DLC), 10.0 mg PPM lyophilized powder was dissolved in 10 mL of HCl (1 M) and stirred in darkness at room temperature for 24 h. Subsequently, the pH was adjusted to neutral with an equimolar amount of NaOH. The concentration of DOX dissociated from PPM was analyzed by HPLC. The DLC was calculated according to the equation, as follows:

$$\text{DLC}(\%) = \left\{ \frac{\text{Weight of loaded DOX in PPM}}{\text{Weight of drug carrier} + \text{Weight of loaded DOX}} \right\} \times 100\%$$

The stability of PPMs was evaluated by monitoring the changes in particle size of polymeric micelles. Simply, PEG_{2K}-SS-CBA-DOX and PEG_{2K}-CBA-DOX PPMs were stored at ambient temperature. The particle size and zeta-potential of the two PPMs were investigated by DLS. Besides, the morphology of PEG_{2K}-SS-CBA-DOX PPM was observed by TEM and SEM. Xigo Acorn Area Particle Interface Analyzer was utilized to determine the relaxation time and specific surface area of PPMs.

pH and Redox Triggered Release of DOX from PPMs

The pH triggered drug release profiles of PEG_{2K}-CBA-DOX, PEG_{2K}-SS-CBA-DOX, PEG_{5K}-CBA-DOX and PEG_{5K}-SS-CBA-DOX PPMs were investigated using a dialysis method at 37°C in phosphate buffer solution (PBS) of pH 7.4 or 5.0, mimicking the physiological

environment or the tumor intracellular environment/microenvironment, respectively. 5 mg of PPMs lyophilized powder were dissolved in corresponding PBS (5 mL) and then transferred into a dialysis tube, immersed in 30 mL of PBS and stirred at 100 rpm in darkness. At certain time intervals, 3 mL of aliquots were pipetted and superseded with fresh PBS. The DOX release was determined using a UV-vis spectrometer and the concentration was calculated accordingly.

The pH and redox dual-triggered DOX release profiles of PEG_{2K}-SS-CBA-DOX and PEG_{5K}-SS-CBA-DOX PPMs were investigated as similar as pH triggered drug release profiles. The release medium was PBS of pH 7.4 or 5.0, mimicking the physiological environment or the tumor intracellular environment/microenvironment, respectively, and PBS of pH 7.4 or 5.0 containing 10 mM GSH, mimicking the physiological environment or tumor intracellular environment under high glutathione concentration, respectively.

Cellular Uptake Assay

Cellular uptake assays of PEG_{2K}-SS-CBA-DOX and PEG_{2K}-CBA-DOX PPMs were evaluated employing A549 cells (Human breast cancer cell). A549 cells were seeded in 24-well plates at a density of 1×10^4 cells/well and incubated at 37°C for 24 h. Then the medium was removed and cells were treated with PEG_{2K}-SS-CBA-DOX/PEG_{2K}-CBA-DOX PPMs at a final DOX concentration of 10 mg/L. After 1, 2 and 4 h of incubation, the cells were fixed with 4% formaldehyde for 10 min, and the nuclei were stained with Hoechst 33258. The cellular uptake of A549 cells was examined using CLSM.

In Vitro Cytotoxicity

For *in vitro* cytotoxicity assay, A549 cells were seeded in 96-well plates at a density of 1×10^4 cells/well and incubated for 24 h. The medium was pipetted, and then cells were incubated with PEG_{2K}-SS-CBA-DOX PPM and PEG_{2K}-CBA-DOX PPM solutions diluted with DMEM at various concentrations for 72 h. Afterward, the drug-containing medium was replaced with the medium containing 10% CCK-8 reagent and the incubation was continued for another 4 h. Finally, the absorbance was measured at 450 nm using a microplate reader.

Pharmacokinetic Evaluation and Tissue Distribution of DOX and PEG_{2K}-SS-CBA-DOX

For pharmacokinetic evaluation, male SD rats were divided randomly into DOX group and PEG_{2K}-SS-CBA-DOX group, and were intravenously injected with DOX and PEG_{2K}-SS-CBA-DOX at DOX dose of 3 mg/kg ($n = 6$). At predetermined time intervals (10, 20, 30 min, 1, 2, 4, 8, 12, 24 h), 0.5 mL blood samples were collected from orbital venous and transferred into a heparinized tube. 0.2 mL plasma was collected after 10 min of centrifugation at 12000 rpm. The samples were treated with 10 μ L of daunorubicin hydrochloride (DNR·HCl) (20 μ g/mL) and 0.5 mL of Tris·HCl (1 M, pH = 9.0). After 3 min of vortex, 5 mL methanol - chloroform (1:2, *v/v*) was added to precipitate proteins. The chloroform phase was collected and dried with nitrogen. Afterwards, the dried mixture was dissolved in 0.2 mL of mobile phase and the supernatant was collected after 10 min of centrifugation (12,000 rpm). Finally, the supernatants were collected for HPLC analysis (Diamonsil C18 (2) column, 5 μ m, 250 \times 4.6 mm, acetonitrile-acidified water (1000 mL contains 1.36 mL of phosphoric acid), 1 mL/min, 35°C, UV = 233 nm).

SD rats were sacrificed after administration of DOX and PEG_{2K}-SS-CBA-DOX PPMs for 2 h. Subsequently, the heart, liver, spleen, lung and kidney were harvested and cut into pieces followed by grinding in 0.5 mL of PBS using tissue grinder. The supernatant was collected after centrifugation at 12000 rpm for 10 min. The supernatant was treated according to the processing method of plasma sample

mentioned. Finally, 150 μ L of treated samples (dissolved in methanol) in black 96-well plates were measured by a Spectra Max M3 multi-function plate reader (Molecular Devices), with the excitation and emission wavelength at 480 and 550 nm, respectively.

To study the distribution of DOX and PEG_{2K}-SS-CBA-DOX micelle in tumors and tissues of tumor-bearing mice, 2×10^6 A549 cells were injected into the left flanks of BALB/c mice to establish xenograft tumor model. When the tumor volume reached 50 mm³, mice were randomly divided into 2 groups ($n = 6$), and intravenously injected with DOX and DiR loaded PEG_{2K}-SS-CBA-DOX micelles (at DOX equivalent 3 mg/kg). At different time intervals after intravenous injection (2, 4, 6 and 12 h), the mice were anesthetized with urethane and monitored using the *in vivo* imaging system. Mice were sacrificed at the last time interval and the heart, liver, spleen, lung, kidney and tumor were collected and analyzed by the *in vivo* imaging system.

Anti-Tumor Efficiency of DOX and PEG_{2K}-SS-CBA-DOX

Tumor-bearing BALB/c mice were randomly divided into 3 groups ($n = 6$). When the tumor reached a volume of 50 mm³, mice were intravenously injected with PBS, DOX and PEG_{2K}-SS-CBA-DOX PPMs at a normalized DOX dose (3 mg/kg) once every three days, respectively. The changes in body weights were monitored. After treatment for 3 weeks, the mice were sacrificed and the tumors were excised for further analysis. The tumor size was measured and the tumor volume was calculated in terms of the formula:

$$V = (\text{length}/\text{width}^2)/2$$

The tumor weight was measured and the tumor inhabitation rate (TIR) was calculated based on:

$$TIR = (1 - \text{tumor weight of treatment group}/\text{tumor weight of control group}) \times 100\%$$

The collected tumors were fixed with 4% formaldehyde solution and stained with hematoxylin and eosin (H&E). The tumor histological study was analyzed on a biological microscope.

Statistical Analysis

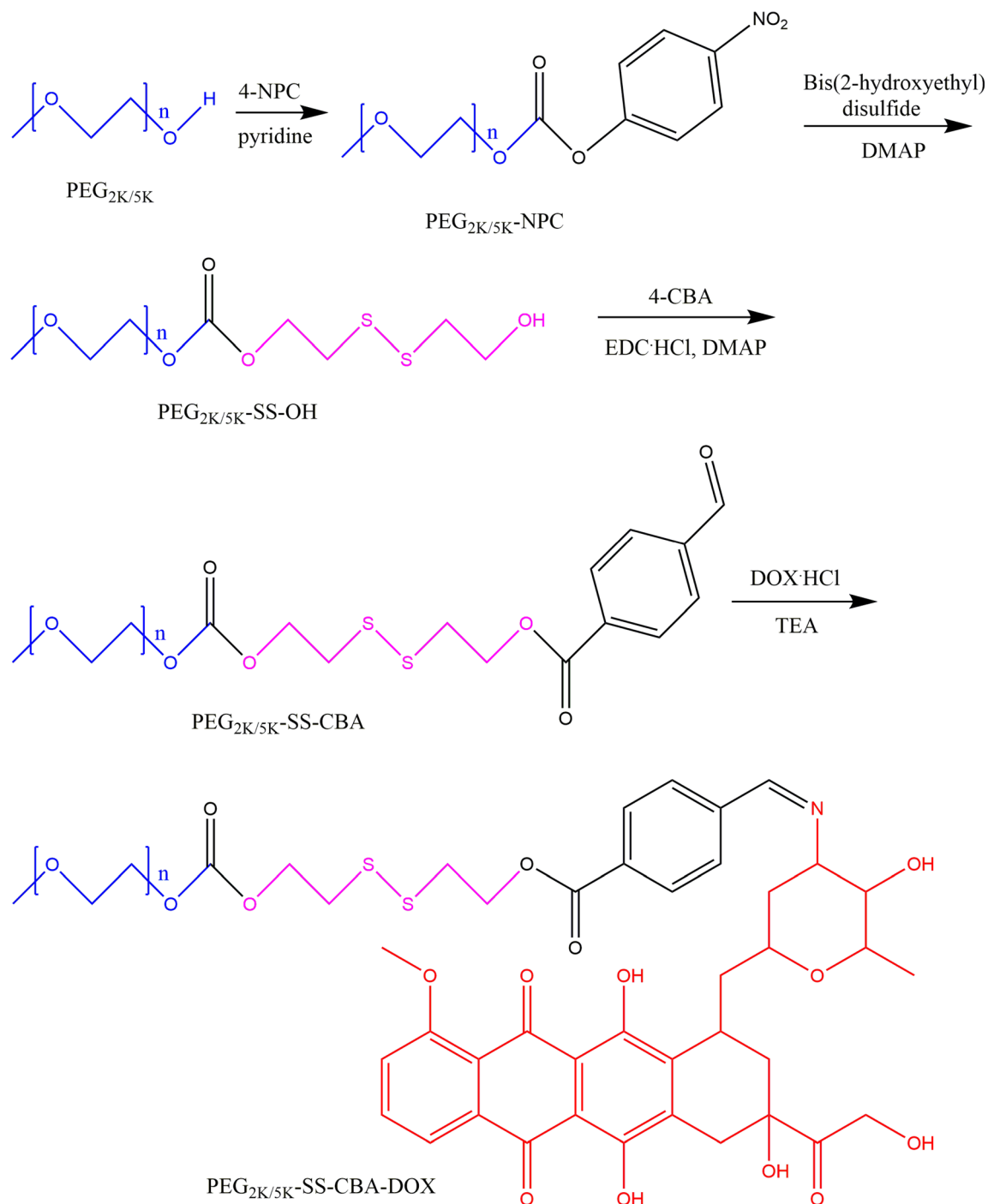
All data were presented as mean \pm standard deviation and examined in parallel three trials. Statistic Package for Social Science (SPSS) software (Version 17.0 for windows) was applied to analyze the processed data. The *p* values obtained according to the Student's *t* test were considered statistically significant difference at $p < 0.05$ and extremely significant difference at $p < 0.01$.

RESULTS AND DISCUSSION

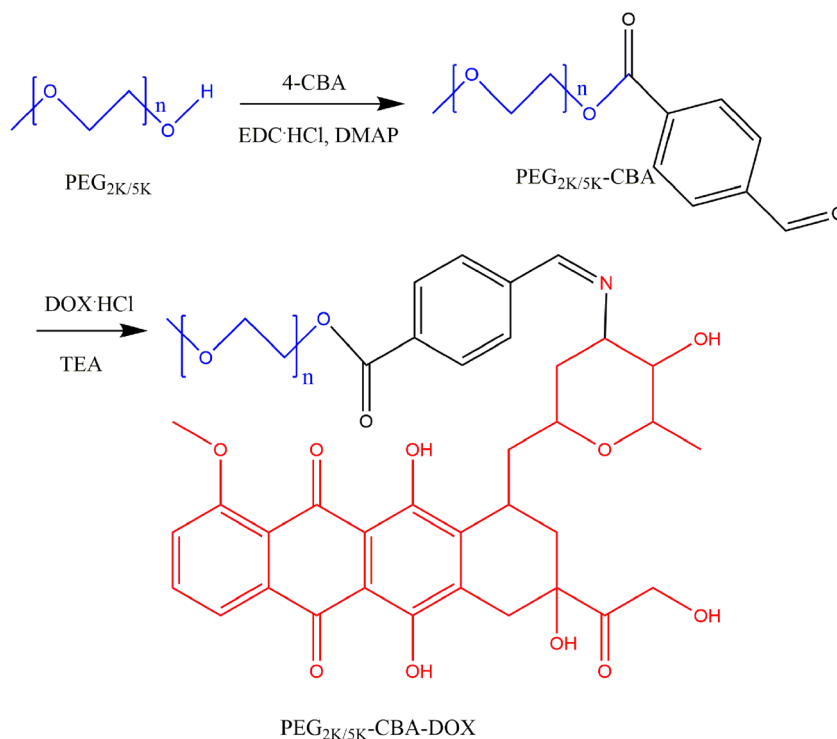
Synthesis and Characterization of Polymeric Prodrug

The synthetic processes of pH/redox dual-sensitive PEG-SS-CBA-DOX and pH-sensitive PEG-CBA-DOX were detailed illustrated in Scheme 1 and Scheme 2. To synthesize PEG-SS-CBA-DOX successfully, PEG-NPC was firstly synthesized by an acylation reaction and confirmed by $^1\text{H-NMR}$ (Fig. S1)

which aromatic proton peaks at 7.39 ppm and 8.28 ppm demonstrated the successful synthesis of desired product. The conversion ratio was calculated to be 100% based on comparing the integrals between the aromatic proton peak at δ 7.39 ppm of 4-NPC and the peak of the repetitive units on PEG at δ 3.48–3.81 ppm (δ 7.39 ppm and 8.28 ppm had the same integral). Next, a transesterification was achieved between PEG-NPC and bis(2-hydroxyethyl) disulfide to yield PEG-SS-OH. The appearance of the aliphatic peaks (2.88 ppm,



Scheme 1 Synthesis of the PEG-SS-CBA-DOX prodrug.

Scheme 2 Synthesis of the PEG-CBA-DOX prodrug.

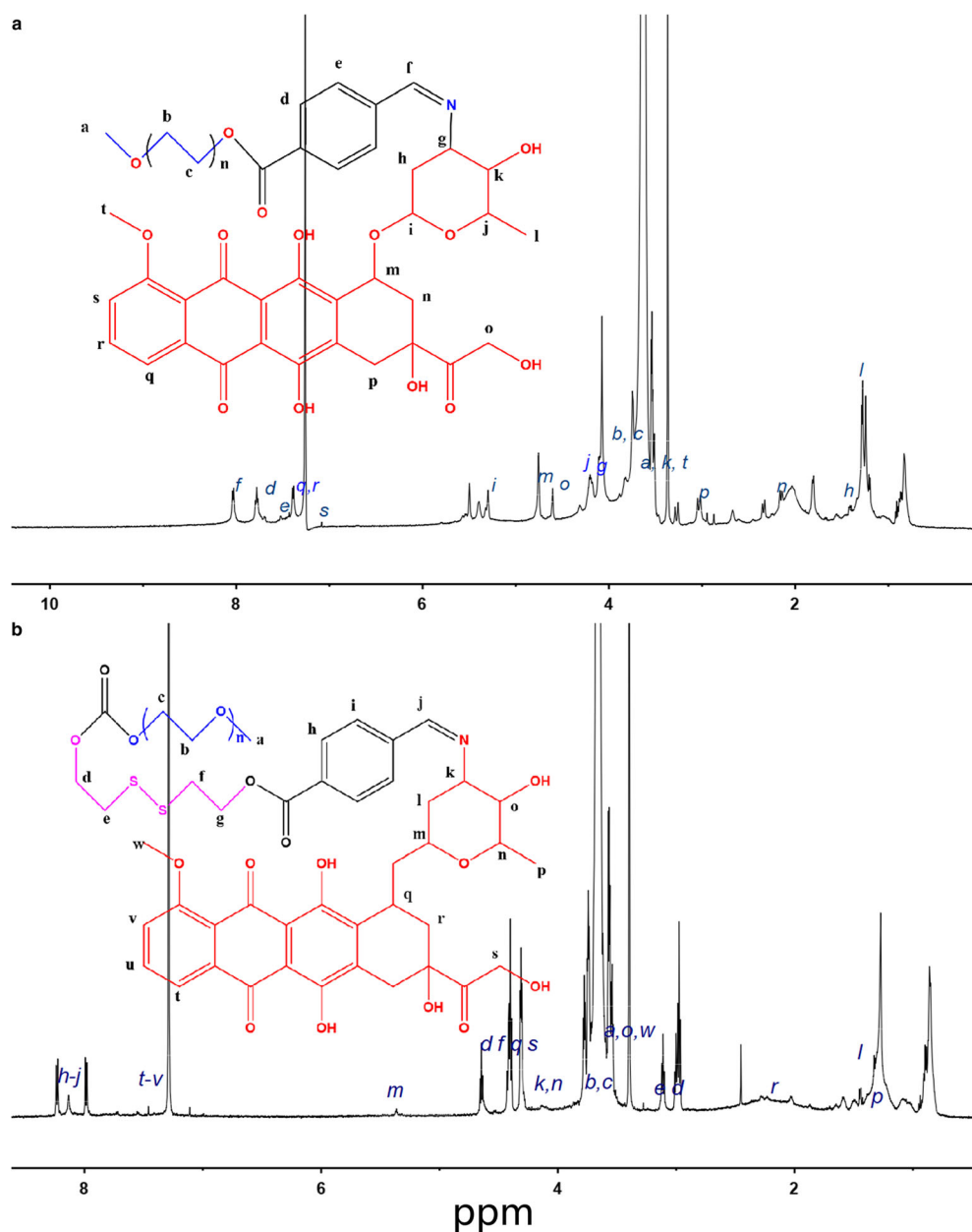
2.96 ppm, 4.29 ppm and 4.39 ppm) were attributed to the bis(2-hydroxyethyl) disulfide of PEG-SS-OH (Fig. S2). The conversion ratio of PEG-SS-OH was calculated to be 93.2% based on the integrals between the new aliphatic proton peak of bis(2-hydroxyethyl) disulfide at δ 2.88 ppm and the peak of the repetitive units on PEG at 3.50–3.89 ppm (δ 2.88 ppm 2.96 ppm, 4.29 ppm and 4.39 ppm had the same integral). Subsequently, PEG-SS-OH and 4-CBA were linked under the catalysis of EDC·HCl and DMAP to introduce the terminal aldehyde group of the polymer molecules. The new aromatic proton peaks of 4-CBA (7.96 ppm, 8.20 ppm) in the ¹H-NMR spectrum of the formed PEG-SS-CBA (Fig. S3) indicated its successful synthesis, and the conversion ratio was calculated to be 88.4% based on the integrals between the aromatic proton peak of 4-CBA at 8.20 ppm and the peak of repetitive units on PEG at 3.50–3.76 ppm. Finally, DOX bound with PEG-SS-CBA easily via the imine bonds. The successful conjugation of DOX to PEG-SS-CBA was confirmed by the appearance of the aromatic proton peaks at δ 7.72/7.56/7.46 ppm of DOX and the imine proton peak at δ 8.13 ppm (Fig. 1B). A high conversion ratio (82.6%) of PEG-SS-CBA-DOX was obtained, according to the imine bond proton peak (8.13 ppm) and the methoxy group proton peak (3.40 ppm). To further confirm the successful synthesis of desired polymers, the FT-IR spectra of the synthesized polymers were measured. The peak of 1747 cm⁻¹ (Fig. 2) was assigned to the -O-C=O bond formed by PEG and bis(2-hydroxyethyl) disulfide. After PEG-SS-CBA combined with DOX, the peak

of ester bond shifted to 1726 cm⁻¹, and a new peak of 1616 cm⁻¹ assigned to imine bond appeared (Fig. 2) (36).

4-CBA was readily conjugated with PEG via an ester bond, which in turn accomplished the transformation of terminal group from hydroxyl to aldehyde group, as illustrated in Scheme 2. The aromatic proton peaks attributed to 4-CBA appeared at δ 7.95 ppm and 8.21 ppm, and the aldehyde group proton peak was at δ 10.10 ppm (Fig. S4). The conversion ratio of PEG-CBA was estimated to be 100.0% according to the integrals between the peak of 4-CBA at δ 7.95 ppm and methoxy group proton peak of PEG at 3.40 ppm. Next, the imine bond was introduced to form the pH-sensitive polymeric prodrug PEG-CBA-DOX. In the ¹H-NMR spectrum of PEG-CBA-DOX (Fig. 1A), the imine bond proton peak appeared at δ 8.04 ppm, the aromatic proton peaks appeared at δ 7.79, 7.43, 7.08 ppm, and the signal peak of DOX was at δ 5.30 ppm. The conversion ratio of PEG-CBA-DOX was calculated to be 96.8% by the integrals between imine bond proton peak and the methoxy group proton peak. The ester bond was formed by PEG and 4-CBA which peak was located at 1724 cm⁻¹ in the FT-IR spectrum (Fig. 2). After the covalent conjugation of PEG-CBA and DOX, a new imine bond absorption peak appeared at 1641 cm⁻¹ (36,37).

The DLC of PPMs were determined by the acid destruction assay and the results displayed that the DOX loading content is 19.5% for PEG_{2K}-SS-CBA-DOX, 20.1% for PEG_{2K}-CBA-DOX, 9.6% for PEG_{5K}-SS-CBA-DOX and 9.4% for PEG_{5K}-CBA-DOX, respectively. The DLC of

Fig. 1 $^1\text{H-NMR}$ spectra of (A) $\text{PEG}_{2\text{K}}\text{-CBA-DOX}$ and (B) $\text{PEG}_{2\text{K}}\text{-SS-CBA-DOX}$.



PPMs formed by $\text{PEG}_{5\text{K}}$ was relatively lower compared with formed by $\text{PEG}_{2\text{K}}$ which was attributed to that up to one molecule of DOX can be attached per molecule of PEG. However, compared to previous studies, the DLC of PPMs composed of $\text{PEG}_{2\text{K}}$ in this study were relatively higher (38,39).

Preparation and Characterization of PPMs

The PPMs were prepared by a simple organic solvent evaporation method. The hydrophilic PEG formed a shell outward and the hydrophobic DOX formed a core inward. $\text{PEG}_{2\text{K}}/\text{5K-SS-CBA-DOX}$ and $\text{PEG}_{2\text{K}}/\text{5K-CBA-DOX}$ micelles were prepared, and $\text{PEG}_{2\text{K}}\text{-SS-CBA-DOX}$ and $\text{PEG}_{2\text{K}}\text{-CBA-DOX}$

DOX PPM were demonstrated in Fig. 3A, which was pink transparent.

The abundant blood vessels, wide gaps between vessel walls and poor structural integrity in solid tumor cause the EPR effect which is perceived as a predominant role in the successful delivery of various nanoparticles (40,41). Therefore, the appropriate particle size of nanocarriers for passively targeting to tumor via EPR effect is crucial for improving drug delivery efficiency. The PEG-SS-CBA-DOX PPMs and the PEG-CBA-DOX PPMs prepared in this study had average diameters of ~ 90 nm and ~ 80 nm, respectively, which made them easy to passively accumulate in tumor tissues. The $\text{PEG}_{2\text{K}}\text{-SS-CBA-DOX}$ PPMs were spherical (Fig. 3B), with the average diameter of ~ 90 nm (Fig. 3C), as supported by the SEM (Fig.

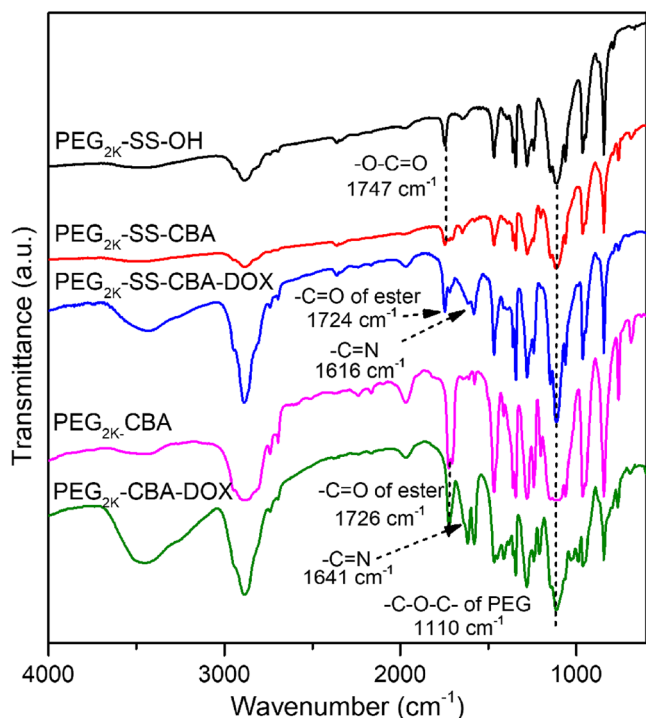


Fig. 2 FT-IR spectrum of various samples during the synthesis.

S7). Meanwhile, the ζ potentials of PEG_{2K}-SS-CBA-DOX PPMs and PEG_{2K}-CBA-DOX PPMs were determined to be -9.45 mV and -11.9 mV, respectively (Fig. S5), which were as electronegative as plasma to remain stable.

The stable of nanomicelles under physiological conditions is greatly warranted for reducing toxicity of chemotherapeutics toward healthy cells, while the “on demand” drug release in short order depends on the timely destruction of nanomicelles in the acidic microenvironment. Hence, the stabilities of PEG_{2K}-SS-CBA-DOX PPMs and PEG_{2K}-CBA-DOX PPMs in aqueous PBS solutions with pH values of 7.4 and 5.0 (physiological conditions and acidic microenvironment) were investigated by measuring the changes in particle size and the relaxation time.

There is no significant difference in particle size changes of the two PPMs within 21 days in a PBS environment of pH 7.4 (Fig. 3D), indicating the excellent stability of the PPMs under normal physiological conditions. However, in a PBS environment of pH 5.0, the particle size of these two PPMs fluctuated significantly within 5 h (Fig. S6), which suggested that the PPMs was broken in the presence of acid environment and this may trigger the simultaneous drug release.

The relaxation time of PEG_{2K}-SS-CBA-DOX PPMs in aqueous solution that were measured by particle interface analyzer to be 2351.4 ms (T_2), with a specific surface area of 0.8 m²/g (Fig. 4). PEG_{5K}-SS-CBA-DOX PPMs had a relaxation time (T_2) of 2163.2 ms with a specific surface area of 1.5 m²/g as depicted. PEG_{2K/5K}-CBA-DOX PPMs displayed the similar relaxation time and specific surface area compared

with PEG_{2K/5K}-SS-CBA-DOX PPMs (Fig. S8). These results showed that the PPMs remained stable and resisted aggregation in aqueous solution (42,43).

pH and Redox Sensitive Release Behavior of PPMs

The drug release behavior of PPMs is not only affected by the environment, but also affected by the molecular weight of nano-carrier (44–47). The dialysis method was applied to investigate the release behaviors of pH-sensitive and pH/redox dual-sensitive PPMs with different molecular weights. Typical PEGs with molecular weights of 2 K and 5 K were used to study the impact of molecular weight on drug release. Respectively, PBS (pH 7.4 and 5.0) were used to mimic the normal physiological environment and the acidic tumor microenvironment. Besides, Good tumor intracellular environment performance was achieved under the simulation in PBS (pH 7.4 and 5.0) containing 10 mM GSH.

As depicted in Fig. 5A, at a lower pH, i.e. pH 5.0, the release of DOX from both PEG_{2K/5K}-SS-CBA-DOX PPMs (37.4% and 23.6% at 72 h) and PEG_{2K/5K}-CBA-DOX PPMs (34.6% and 16.7% at 72 h) was significantly faster compared with at the pH value of 7.4 (27.7%, 12.6%, 26.2% and 10.8% at 72 h, respectively), which could be ascribed to the cleavage of acid-labile imine bond. Meanwhile, when treated with PBS of 5.0 with 10 mM of GSH, the cumulative release of DOX from PEG_{2K/5K}-SS-CBA-DOX PPMs was as efficient as to be 84.9% in 72 h (Fig. 5B). Numerous studies have shown that the disulfide bond can be broken easily in the presence of high concentrations of GSH (19,48–50). The cumulative release of DOX from PPMs at pH 5.0 with 10 mM GSH is two times higher than that at pH 5.0, which mainly because the PPMs were dissociated under high-concentration of GSH, resulting in the prodrug easier to react with H⁺ in the tumor acidic microenvironment, thereby accelerating the drug release. The dissociation of PPMs was dramatically accelerated under the condition of acid and high concentration of GSH, resulting in the rapid shedding of DOX from PPMs. Next, the drug release behavior under physiological environment (pH 7.4) with high concentrations of GSH was also quantified. The cumulative release of DOX from PEG_{2K/5K}-SS-CBA-DOX PPMs under pH 7.4 with 10 mM of GSH (41.9% and 24.4% at 72 h, respectively) was almost two times higher than that under pH 7.4 (27.7% and 12.6% at 72 h, respectively), which indicated that the unique high GSH concentration in tumor microenvironment can accelerate the drug release from PEG_{2K/5K}-SS-CBA-DOX PPMs despite of the extra or intra pH values of tumor tissues (51,52).

The cumulative release profile of DOX from the PPMs with the same stimuli-responsive bonds exhibited negative correlation with the molecular weight of PEG under the same release medium (Fig. 5). According to the previous report (37), the higher the curling degree of polymers, the slower the drug diffuses from

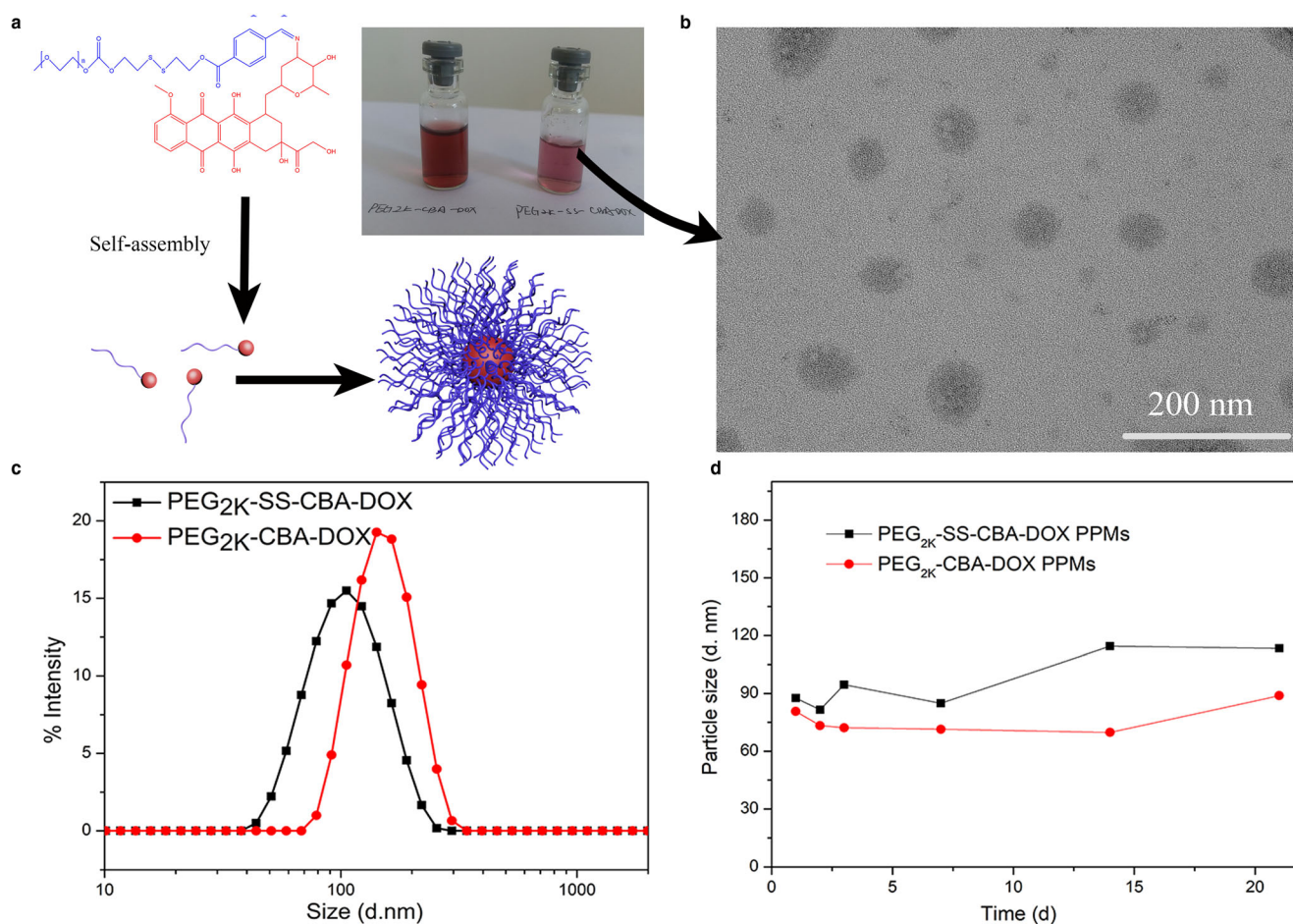


Fig. 3 (A): PEG_{2K}-CBA-DOX and PEG_{2K}-SS-CBA-DOX micelles at a concentration of 0.5 mg/mL; (B): TEM image of PEG_{2K}-SS-CBA-DOX micelles; (C): Size distribution of PEG_{2K}-CBA-DOX and PEG_{2K}-SS-CBA-DOX micelles at a concentration of 0.5 mg/mL; (D): Stability of micelles of PEG_{2K}-CBA-DOX and PEG_{2K}-SS-CBA-DOX in pH 7.4 PBS at room temperature.

the micelles. This provides a powerful tool to control drug release via adjusting the molecular weight of drug carrier.

Cellular Uptake of PPMs

The PPMs composed of PEG_{2K} possessed relatively higher DLC and exhibited improved *in vitro* drug release behaviors compared with PPMs based on PEG_{5K}. We measured the cellular uptake of PEG_{2K}-SS-CBA-DOX PPMs and PEG_{2K}-CBA-DOX PPMs in A549 cells using CLSM. As illustrated in Fig. 6, cells co-incubated with the two PPMs exhibited convenient cellular internalization that may be achieved through membrane fusion pathways under the unique shell-core structure of micelles. PEG_{2K}-SS-CBA-DOX PPMs showed stronger red fluorescence intensity at 1 h. As time elapsed, the red fluorescence intensity of cells incubated with two PPMs gradually increased and tended to be equal. This may be related to PEG_{2K}-SS-CBA-DOX PPMs being able to show a stronger red fluorescence intensity at 1 h when fluorescent DOX was faster dissociated from PEG_{2K}-SS-CBA-DOX PPMs compared to PEG_{2K}-CBA-DOX PPMs after the two PPMs were

internalized by tumor cells. Gradually, released DOX from PPMs reached the peak in tumor cells so that the fluorescence intensity tended to be equal.

Difference fluorescence intensity in earlier stage of the two PPMs in A549 cells can be attributed to the destruction of disulfide due to the high concentration of GSH in cancer cells. As reported previously (53), the decrease of GSH concentration owing to the existence of disulfide can alleviate the excretion of chemotherapeutics. Therefore, our results demonstrated that the prepared PEG_{2K}-SS-CBA-DOX PPM provided a novel insight in developing new drug delivery system to conquer the multi-drug resistance (MDR). Subsequent phenomena about the equalization of fluorescence intensity indicated that PPMs can be effectively internalized by cells. Collectively, these observations strongly implied that the pH/redox stimuli-responsive PPM showed favorable cellular internalization.

Anti-Tumor Activities *In Vitro*

The *in vitro* cytotoxicity of PEG_{2K}-SS-CBA-DOX, PEG_{2K}-CBA-DOX and free DOX was evaluated using the CCK-8

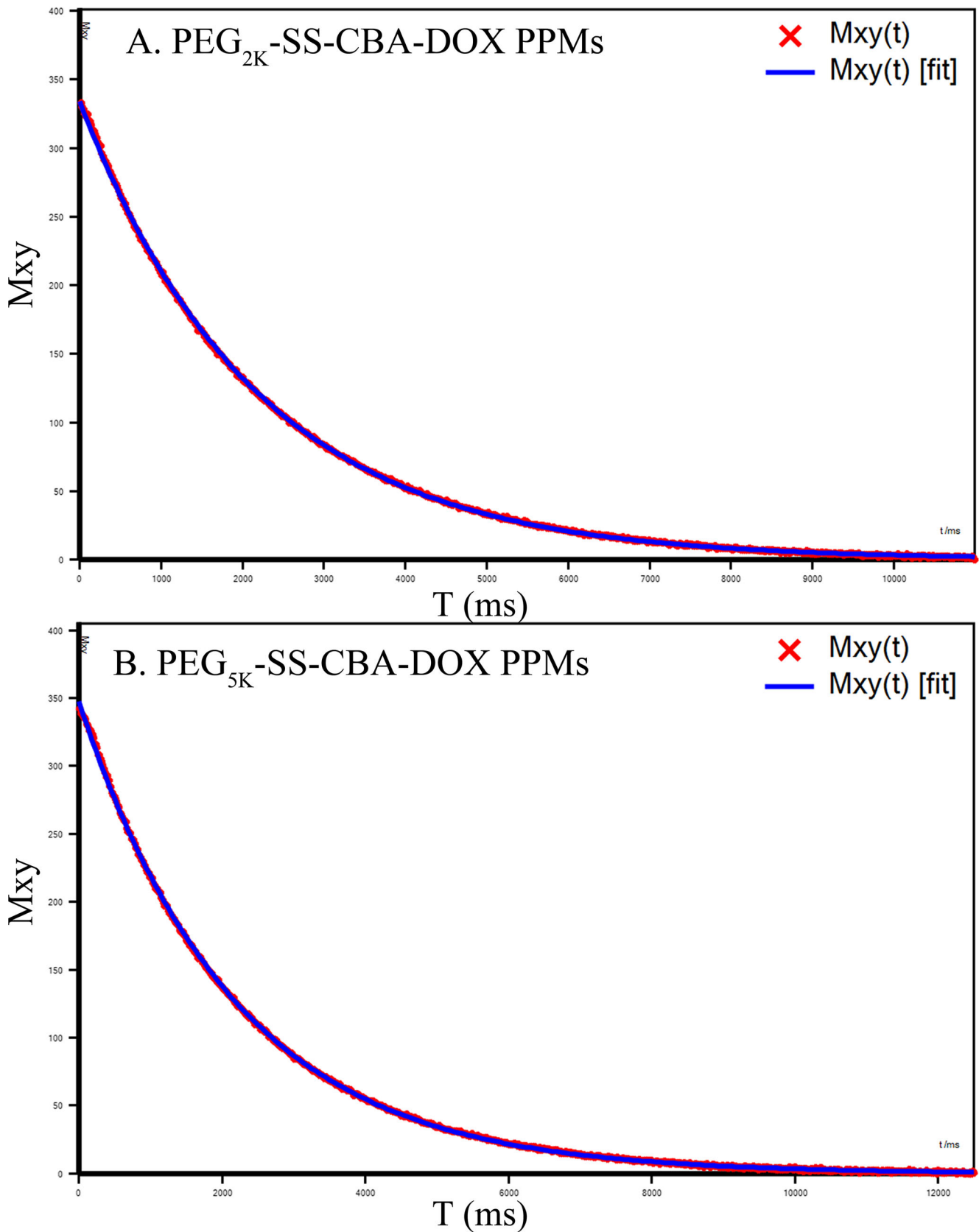
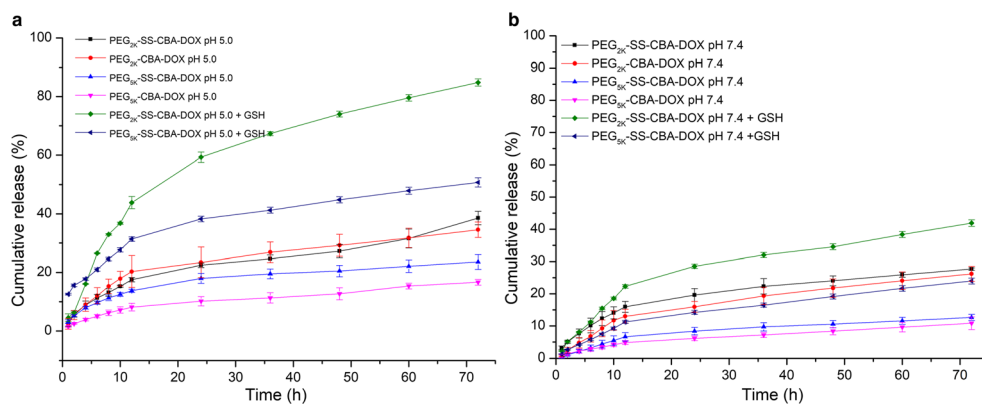


Fig. 4 Surface area measurements of PEG_{2K}-SS-CBA-DOX PPMs (A) and PEG_{5K}-SS-CBA-DOX PPMs (B) at a concentration of 1 mg/mL measured using a Xigo Acom Area Particle Interface Analyzer. M_{xy} is the transverse magnetization vector.

Fig. 5 Cumulative release of DOX from various PPMs at pH 5.0 and 7.4 (A); Cumulative release of DOX from various PPMs at pH 5.0 and 7.4 with 10 mM of GSH (B).



method (Fig. 7). A number of researches indicated that drugs exhibited reduced cytotoxicity after loading onto polymers (54,55). PEG_{2K}-SS-CBA-DOX PPMs exhibited slightly higher cytotoxicity against A549 cell lines compared with PEG_{2K}-CBA-DOX PPMs (IC_{50} 7.71 μ g/mL vs 31.97 μ g/mL), which could be attributed to the faster destruction of dual-sensitive PPMs. However, the IC_{50} of these two synthesized PPMs was much higher than free DOX (IC_{50} 0.37 μ g/mL). This phenomenon was most likely ascribed to the slow internalization and subsequent intracellular dissociation of the nanoparticles.

Pharmacokinetic Study of DOX and PEG_{2K}-SS-CBA-DOX Micelles

The blood concentration and half-time of drug have an important influence on the therapy efficiency. As reported, DOX is cleared quickly in systemic circulation (56,57), which is consistent with Fig. 8A. PEG_{2K}-SS-CBA-DOX micelles exhibited an “oral-like” blood concentration curve. Promisingly, the area-under the curve (AUC) of DOX from PEG_{2K}-SS-CBA-DOX PPMs was increased by 2.68 times compared with free DOX (Table I). DOX dissociated from PPMs because the PPMs were destroyed by enzymes in the tissues, such as the liver, and thus triggered the concurrent drug release. DOX was almost completely depleted by the body after treating with free DOX for 12 h. The $t_{1/2}$ of PPMs camouflaged DOX were increased by 1.45 folds when compared with free DOX, which illustrated that PPMs can effectively extend the half-life of DOX.

Tissue Toxicity and Tissue Distribution of DOX and PPMs

DOX has severe cardiotoxicity, nephrotoxicity and myelosuppression although it is widely used in clinical (58,59). To investigate the tissue toxicity of PPMs, we analyzed the distribution of DOX and PPMs in the tissues of SD rats. As depicted in Fig. 8B, DOX is more easily trapped in the

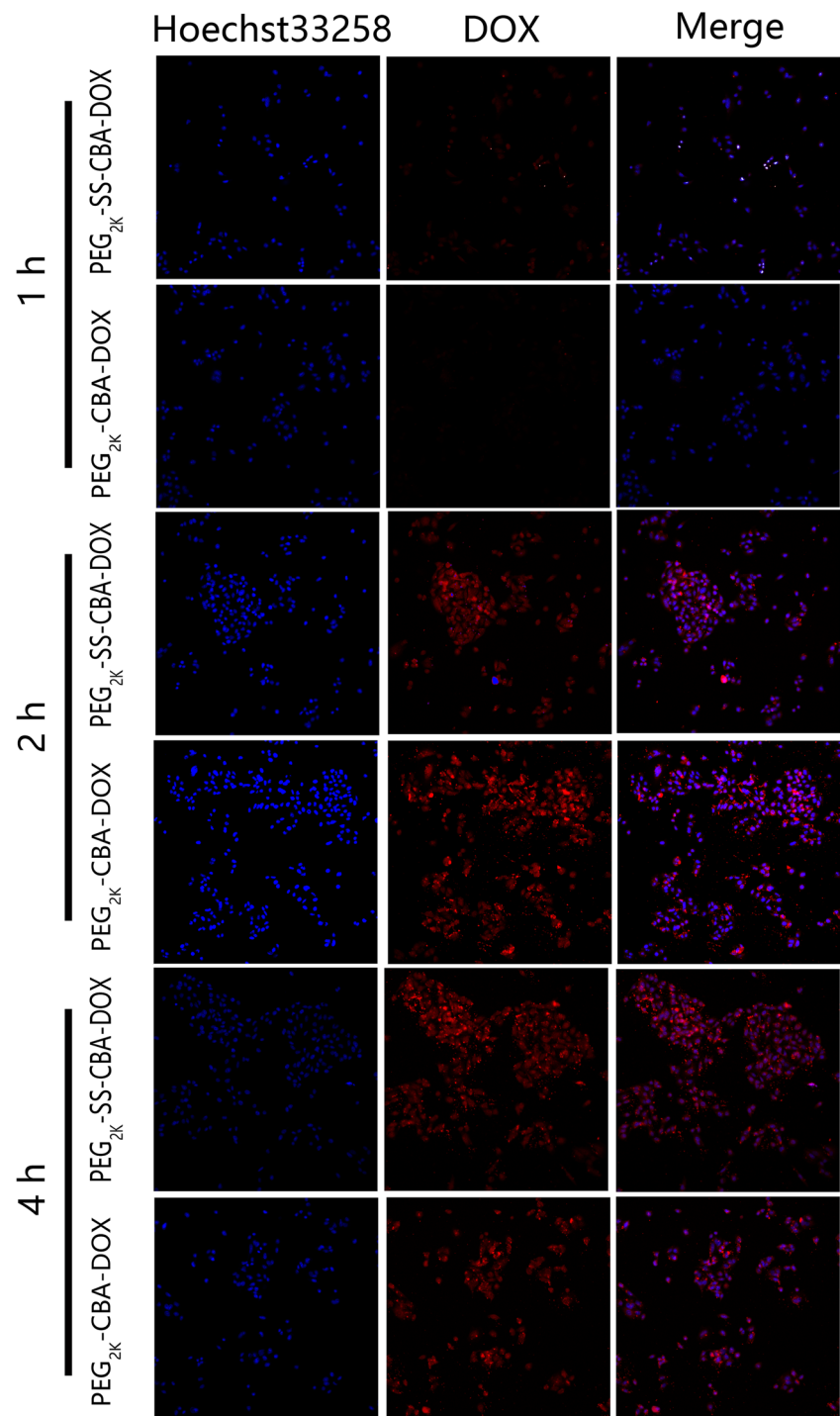
heart compared with the PPMs after 2 h intravenous injection, indicating its severe cardiotoxicity. Besides, the free DOX accumulated in the organs (except for the spleen) was higher than that of PPMs. The reduced distribution of DOX loaded in PPM in most major organs resulted in a decrease in the toxicity of DOX to normal tissues, therefore reduced side effects.

To study the distribution law of DOX and PPMs in the main organs and tumor, an *in vivo* living imaging system was employed. Both DOX and PEG_{2K}-SS-CBA-DOX micelles were rapidly distributed in mice after intravenous injection. Over time, DOX was rapidly cleared by the body (Fig. 8C). However, the clearance rate of PEG_{2K}-SS-CBA-DOX micelles was much slower than that of DOX, and PEG_{2K}-SS-CBA-DOX micelles gradually accumulated at the tumor site (Fig. 8C and D). The reasonable particle size (~90 nm) design of the prepared micelles is a critical strategy to ensure that the PPMs can effectively penetrate various barriers and accumulate in tumor. In addition, the PEG endows the PPMs with a prolonged blood circulation, which also improves the accumulation of PPMs in tumor indirectly.

Anti-Tumor Efficiency and Histological Analysis

To verify the enhanced antitumor efficiency of tumor microenvironment stimuli-responsive PPMs, the pharmacodynamic assay was performed on A549 tumor-bearing BALB/c mice. The DOX group and PEG_{2K}-SS-CBA-DOX group had therapeutic effect to some extent compared with the control group (PBS group). The tumor volumes were significantly decreased in the PEG_{2K}-SS-CBA-DOX group compare with DOX group after treatment for 21 days (Table II). Similarly, the tumor weights were tremendously reduced, which leads to an increase in tumor inhibition rate as illustrated in Table II, Fig. 9 A and D. The tumor volumes and weights of PEG_{2K}-SS-CBA-DOX group were greatly reduced compared with DOX group, which implied that the PPMs with pH and redox-sensitive tumor microenvironment responsiveness can achieve long-

Fig. 6 Cellular uptake of PEG_{2K}-SS-CBA-DOX (A) and PEG_{2K}-CBA-DOX (B) PPMs. Blue fluorescence represents cell nucleus stained by Hoechst 33258, red fluorescence represents DOX internalized by cells.



term circulation *in vivo*, avoid rapid elimination and improve the accumulation in tumor sites, thereby enhancing the anti-tumor efficiency. The results of anti-tumor efficiency tests in combination with the results of the cytotoxicity tests and the biodistribution tests indicated that the systemic toxicity of PEG_{2K}-SS-CBA-DOX was significantly reduced in comparison with DOX. Body weight changes

of tumor-bearing mice in Fig. 9B verified this result. As for histological study, tumor tissues in the DOX group and PEG_{2K}-SS-CBA-DOX PPMs group displayed different degrees of necrosis (Fig. 9E) based on the proportion of tumor cell necrosis compared with the PBS group, and an obviously higher degree of tumor necrosis phenomenon was observed in the PEG_{2K}-SS-CBA-DOX PPMs group.

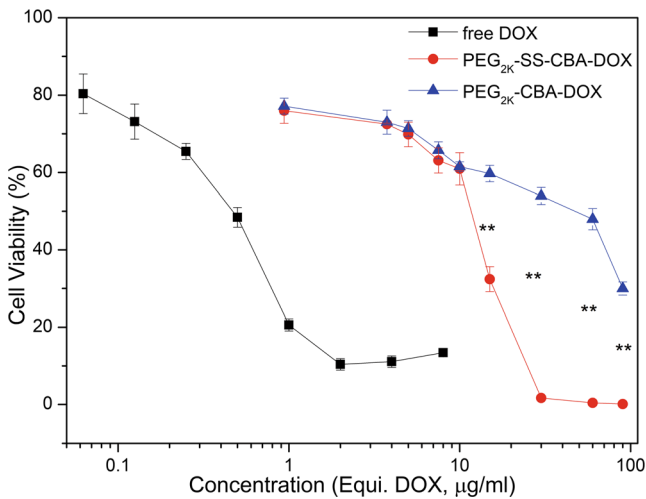


Fig. 7 Cell viability of PEG_{2K}-SS-CBA-DOX, PEG_{2K}-CBA-DOX and free DOX at a DOX equivalent. **, *p* < 0.01, extremely significant difference.

The improved long-term circulation and the EPR effect which depended on particle size play important roles in the cancer treatment of PEG_{2K}-SS-CBA-DOX PPMs which can accumulate in the tumor site and release DOX rapidly, thereby maximizing desired effects of drug.

Table 1 The Pharmacokinetic Parameter of DOX and PEG_{2K}-SS-CBA-DOX PPMs in SD Rats

Group	AUC (mg/L*h)	MRT (h)	t _{1/2} (h)
DOX	890.79 ± 95.41	4.60 ± 0.19	12.94 ± 8.95
PEG _{2K} -SS-CBA-DOX	2388.07 ± 218.31	9.64 ± 1.13	18.72 ± 14.17

CONCLUSIONS

The predominant strategy for this research is suitable particle size of PPMs works in tandem with tumor microenvironment stimuli-responsiveness (pH/redox dual-sensitive) to improve therapeutic outcome and reduce side effects of chemotherapeutics. The prepared prodrug with considerable specific surface area is capable of self-assembling into micelles with appropriate particle size to achieve the passive targetability via EPR effect. The accelerated drug release in acidic/reductive tumor microenvironments enables the PPMs advantages in terms of improving chemotherapeutic efficacy. We proposed a strategy to control the drug release of polymeric prodrugs based on controlling the molecular weight of polymers. Furthermore, the results of cellular uptake and cytotoxicity

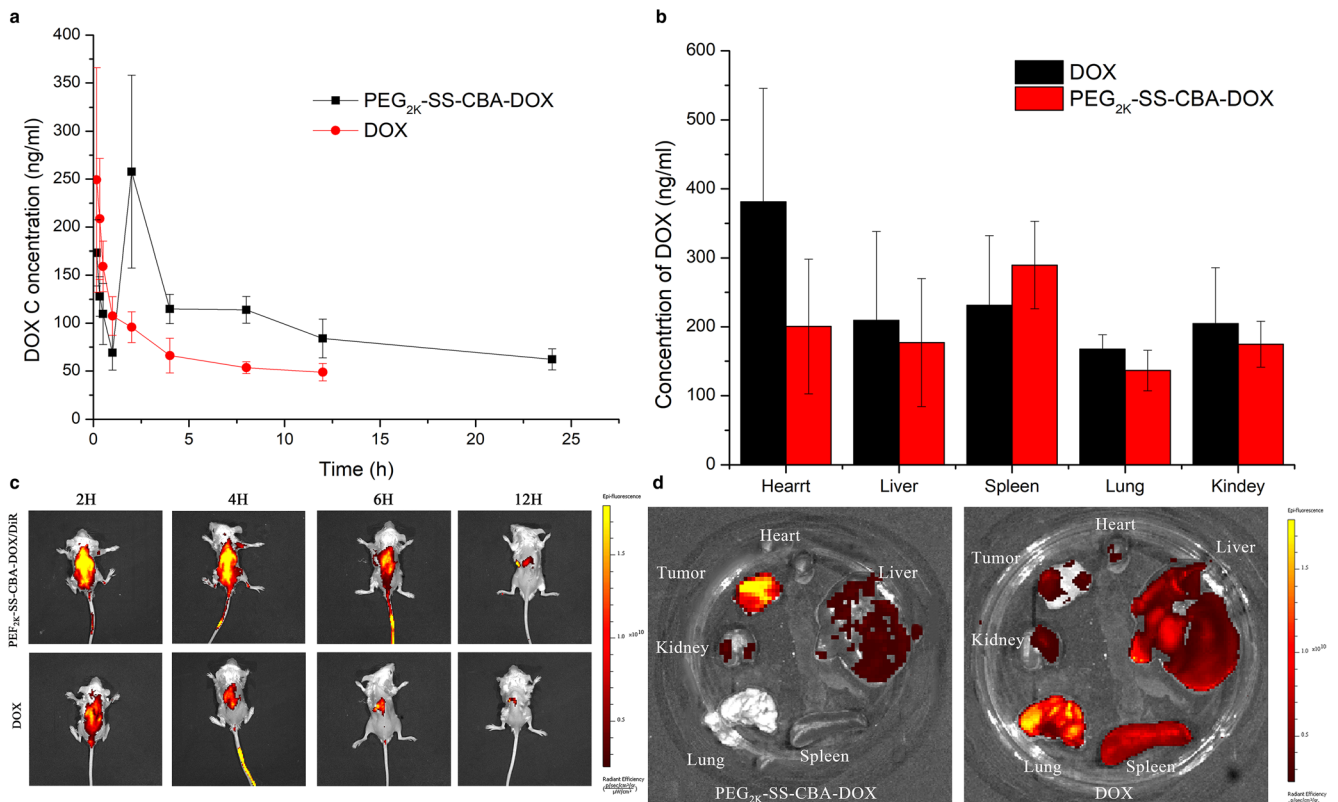


Fig. 8 Pharmacokinetic study and biodistribution of DOX and PEG_{2K}-SS-CBA-DOX PPMs. (A): Pharmacokinetic curve of DPX and PEG_{2K}-SS-CBA-DOX PPMs; (B): Tissue distribution of DOX and PEG_{2K}-SS-CBA-DOX PPMs in SD rats; (C): The distribution over time after tail vein injection of DOX and PEG_{2K}-SS-CBA-DOX/DIR PPMs in mice; (D): Tissue and tumor distribution of DOX and PEG_{2K}-SS-CBA-DOX/DIR PPMs after 12 h of post administration.

Table II Tumor Weight, Volume and Tumor Growth Inhibition Rate After 21 d of Treatment

Group	Tumor Weight (g)	Tumor Volume (mm ³)	Tumor Growth Inhibition Rate (%)
PBS	0.53 ± 0.08	731.83 ± 257.56	–
DOX	0.31 ± 0.07**	429.92 ± 77.36*	41.94 ± 6.08
PEG _{2k} -SS-CBA-DOX	0.14 ± 0.06**	216.17 ± 109.69**	74.60 ± 7.76**

Values represent mean ± S.D. (n = 6).

*, $p < 0.05$, significant difference; **, $p < 0.01$, extremely significant difference

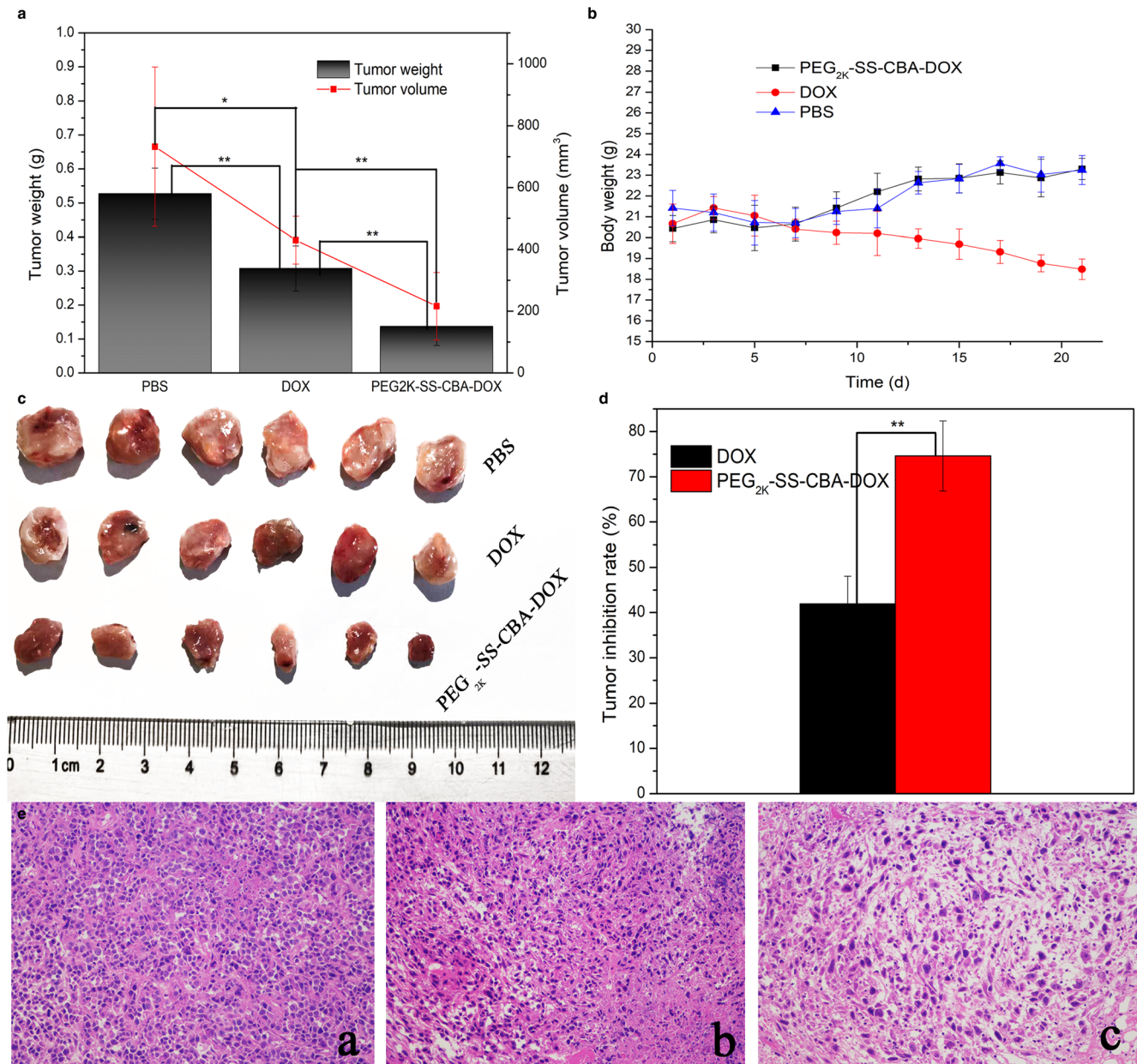


Fig. 9 Antitumor efficiency and histological analysis of DOX and PEG_{2k}-SS-CBA-DOX PPMs. (A): Tumor weight and volume after 21 d treatment; (B): Changes in body weight of mice during treatment; (C): Photographs of tumors; (D): Tumor inhibition rate of DOX and PEG_{2k}-SS-CBA-DOX PPMs after 21 d of treatment; (E): Histological analysis of tumors of mice 21 d of post administration of PBS (a), DOX (b) and PEG_{2k}-SS-CBA-DOX PPMs (c). *, $p < 0.05$, significant difference, **, $p < 0.01$, extremely significant difference.

assays revealed that the prepared PPMs can be efficiently internalized by tumor cells and reduce the side effects of DOX. The “oral-like” drug concentration-time profiles, biodistribution, tissue distribution, anti-tumor efficiency and histological study revealed that the prepared dual-sensitive PPMs are superior in improving *in vitro* and *in vivo* release pharmacokinetics, enhancing anti-tumor therapeutic effect and reducing side effects of DOX.

ACKNOWLEDGEMENTS AND DISCLOSURES

The authors are grateful to Anning Li from Wuya College of Innovation, Shenyang Pharmaceutical University, China, Dr. Shugang Qin and Overby Madison from University of North Dakota, USA for their assistance with writing this paper.

Funding

This work was supported by the Disruptive Technologies Innovation Fund of Shenyang Pharmaceutical University (DFJJ2018208), the Natural Science Foundation of Liaoning Province of China (Grant No.201602706), the Liaoning S&T Project (2014226032), the Scientific Research General Project of Liaoning Provincial Department of Education (201610163 L29) and the National Natural Science Foundation of China (81502927 and 81603053).

COMPLIANCE WITH ETHICAL STANDARDS

Declaration of Interest The authors report no conflicts of interest. The authors alone are responsible for the content and writing of this article.

REFERENCES

- Ganipineni LP, Danhier F, Preat V. Drug delivery challenges and future of chemotherapeutic nanomedicine for glioblastoma treatment. *J Control Release*. 2018;281:42–57.
- Han J, Zhao D, Li D, Wang X, Jin Z, Zhao K. Polymer-based nanomaterials and applications for vaccines and drugs. *Polymers*. 2018;10(1).
- Wang C, Zhang Z, Chen B, Gu L, Li Y, Yu S. Design and evaluation of galactosylated chitosan/graphene oxide nanoparticles as a drug delivery system. *J Colloid Interface Sci*. 2018;516:332–41.
- Zeng Z, Wei Z, Ma L, Xu Y, Xing Z, Niu H, et al. pH-responsive nanoparticles based on ibuprofen prodrug as drug carriers for inhibition of primary tumor growth and metastasis. *J Mater Chem B*. 2017;5(33):6860–8.
- Hou S, Yang Y, Zhou S, Kuang X, Yang Y, Gao H, et al. Novel SS-31 modified liposomes for improved protective efficacy of minocycline against drug-induced hearing loss. *Biomater Sci*. 2018;6(6):1627–35.
- Park K. Drug release mechanisms from amorphous solid dispersions. *J Control Release*. 2015;211:171–1.
- Climont N, Garcia I, Marradi M, Chiodo F, Miralles L, Jose Maleno M, et al. Loading dendritic cells with gold nanoparticles (GNPs) bearing HIV-peptides and mannosides enhance HIV-specific T cell responses. *Nanomed-Nanotechnol Biol Med*. 2018;14(2):339–51.
- Lin Y-S, Haynes CL. Impacts of mesoporous silica nanoparticle size, pore ordering, and pore integrity on hemolytic activity. *J Am Chem Soc*. 2010;132(13):4834–42.
- Sohaebuddin SK, Thevenot PT, Baker D, Eaton JW, Tang L. Nanomaterial cytotoxicity is composition, size, and cell type dependent. *Particle Fibre Toxicol*. 2010;7.
- Duan X, Chen H, Fan L, Kong J. Drug self-assembled delivery system with dual responsiveness for Cancer chemotherapy. *ACS Biomater Sci Eng*. 2016;2(12):2347–54.
- Stenstrom P, Hjorth E, Zhang Y, Andren OCJ, Guette-Marquet S, Schultzberg M, et al. Synthesis and in vitro evaluation of monodisperse amino-functional polyester dendrimers with rapid degradability and antibacterial properties. *Biomacromolecules*. 2017;18(12):4323–30.
- Suk JS, Xu Q, Kim N, Hanes J, Ensign LM. PEGylation as a strategy for improving nanoparticle-based drug and gene delivery. *Adv Drug Deliv Rev*. 2016;99:28–51.
- Li J, Li Y, Wang Y, Ke W, Chen W, Wang W, et al. Polymer prodrug-based Nanoreactors activated by tumor acidity for orchestrated oxidation/chemotherapy. *Nano Lett*. 2017;17(11):6983–90.
- Yu H-Y, Wang C, Abdalkarim SYH. Cellulose nanocrystals/polyethylene glycol as bifunctional reinforcing/compatibilizing agents in poly(lactic acid) nanofibers for controlling long-term in vitro drug release. *Cellulose*. 2017;24(10):4461–77.
- Yu X, Gao D, Gao L, Lai J, Zhang C, Zhao Y, et al. Inhibiting metastasis and preventing tumor relapse by triggering host immunity with tumor-targeted photodynamic therapy using photosensitizer-loaded functional Nanographenes. *ACS Nano*. 2017;11(10):10147–58.
- Sun H, Guo B, Cheng R, Meng F, Liu H, Zhong Z. Biodegradable micelles with sheddable poly(ethylene glycol) shells for triggered intracellular release of doxorubicin. *Biomaterials*. 2009;30(31):6358–66.
- Liu C, Zhu X, Duan J, Liang X, Li X, Yang J. Hydrogen peroxide-responsive peroxalate ester-linked PCL-PEG micelles as drug carrier. *J Control Release*. 2017;259:E17–7.
- Sun X, Wang G, Zhang H, Hu S, Liu X, Tang J, et al. The blood clearance kinetics and pathway of polymeric micelles in Cancer drug delivery. *ACS Nano*. 2018;12(6):6179–92.
- Zhu C, Li Y. PEG-sheddable reduction-sensitive polyurethane micelles for triggered intracellular anti-tumor drug delivery. *J Control Release*. 2017;259:E14–5.
- Wu M, Li J, Lin X, Wei Z, Zhang D, Zhao B, et al. Reduction/photo dual-responsive polymeric prodrug nanoparticles for programmed siRNA and doxorubicin delivery. *Biomater Sci*. 2018;6(6):1457–68.
- Wan Z, Sun J, Xu J, Moharil P, Chen J, Xu J, et al. Dual functional immunostimulatory polymeric prodrug carrier with pendent indoximod for enhanced cancer immunochemotherapy. *Acta Biomater*. 2019;90:300–13.
- He X, Cai K, Zhang Y, Lu Y, Guo Q, Zhang Y, et al. Dimeric prodrug self-delivery nanoparticles with enhanced drug loading and bioreduction responsiveness for targeted Cancer therapy. *ACS Appl Mater Interfaces*. 2018;10(46):39455–67.
- Buwalda S, Al Samad A, El Jundi A, Bethry A, Bakkour Y, Coudane J, et al. Stabilization of poly(ethylene glycol)-poly(epsilon-caprolactone) star block copolymer micelles via aromatic groups for improved drug delivery properties. *J Colloid Interface Sci*. 2018;514:468–78.
- Jafarzadeh-Holagh S, Hashemi-Najafabadi S, Shaki H, Vashghani-Farahani E. Self-assembled and pH-sensitive mixed micelles as an intracellular doxorubicin delivery system. *J Colloid Interface Sci*. 2018;523:179–90.

25. Yin T, Wang Y, Chu X, Fu Y, Wang L, Zhou J, et al. Free Adriamycin-loaded pH/reduction dual-responsive hyaluronic acid-Adriamycin prodrug micelles for efficient Cancer therapy. *ACS Appl Mater Interfaces*. 2018;10(42):35693–704.
26. Sun J, Liu Y, Chen Y, Zhao W, Zhai Q, Rathod S, et al. Doxorubicin delivered by a redox-responsive dasatinib-containing polymeric prodrug carrier for combination therapy. *J Control Release : Off J Control Release Soc*. 2017;258:43–55.
27. Ma B, Zhuang W, Wang Y, Luo R, Wang Y. pH-sensitive doxorubicin-conjugated prodrug micelles with charge-conversion for cancer therapy. *Acta Biomater*. 2018;70:186–96.
28. Zhou W, Li C, Wang Z, Zhang W, Liu J. Factors affecting the stability of drug-loaded polymeric micelles and strategies for improvement. *J Nanoparticle Res*. 2016;18(9).
29. Gao H, Liu J, Yang C, Cheng T, Chu L, Xu H, et al. The impact of PEGylation patterns on the in vivo biodistribution of mixed shell micelles. *Int J Nanomedicine*. 2013;8:4229–46.
30. H-j H, Han Y, Cheong M, Kral P, Hong S. Dendritic PEG outer shells enhance serum stability of polymeric micelles. *Nanomed-Nanotechnol Biol Med*. 2018;14(6):1879–89.
31. Bai S, Ahsan F. Synthesis and evaluation of Pegylated Dendrimeric Nanocarrier for pulmonary delivery of low molecular weight heparin. *Pharm Res*. 2009;26(3):539–48.
32. Lin D, Jiang Q, Cheng Q, Huang Y, Huang P, Han S, et al. Polycation-detachable nanoparticles self-assembled from mPEG-PCL-g-SS-PDMAEMA for in vitro and in vivo siRNA delivery. *Acta Biomater*. 2013;9(8):7746–57.
33. Ma Y, Fan X, Li L. pH-sensitive polymeric micelles formed by doxorubicin conjugated prodrugs for co-delivery of doxorubicin and paclitaxel. *Carbohydr Polym*. 2016;137:19–29.
34. Luo C, Sun J, Liu D, Sun B, Miao L, Musetti S, et al. Self-assembled redox dual-responsive prodrug-Nanosystem formed by single Thioether-bridged paclitaxel-fatty acid conjugate for Cancer chemotherapy. *Nano Lett*. 2016;16(9):5401–8.
35. N'Da DD, Breytenbach JC. Synthesis of methoxypoly(ethylene glycol) carbonate prodrugs of zidovudine and penetration through human skin in vitro. *J Pharm Pharmacol*. 2009;61(6):721–31.
36. Bingul M, Tan O, Gardner CR, Sutton SK, Arndt GM, Marshall GM, Cheung BB, Kumar N, Black DS. Synthesis, Characterization and Anti-Cancer Activity of Hydrazide Derivatives Incorporating a Quinoline Moiety. *Molecules*. 2016;21(7).
37. Rao KSVK, Zhong Q, Bielski ER, da Rocha SRP. Nanoparticles of pH-responsive, PEG-doxorubicin conjugates: interaction with an in vitro model of lung adenocarcinoma and their direct formulation in propellant-based portable inhalers. *Mol Pharm*. 2017;14(11):3866–78.
38. Saw PE, Yao H, Lin C, Tao W, Farokhzad OC, Xu X. Stimuli-responsive polymer-prodrug hybrid nanoplatfor for multistage siRNA delivery and combination cancer therapy. *Nano Lett*. 2019.
39. Pan X, Chen J, Yang M, Wu J, He G, Yin Y, et al. Enzyme/pH dual-responsive polymer prodrug nanoparticles based on 10-hydroxycamptothecin-carboxymethylchitosan for enhanced drug stability and anticancer efficacy. *Eur Polym J*. 2019;117:372–81.
40. Nakamura H, Koziolova E, Chytil P, Etrych T, Haratake M, Maeda H. Superior penetration and cytotoxicity of HPMA copolymer conjugates of Pirarubicin in tumor cell spheroid. *Mol Pharm*. 2019;16(8):3452–9.
41. Fang J, Islam R, Islam W, Yin H, Subr V, Etrych T, Ulbrich K, Maeda H. Augmentation of EPR Effect and Efficacy of Anticancer Nanomedicine by Carbon Monoxide Generating Agents. *Pharmaceutics*. 2019;11(7).
42. Verma V, Balasubramanian K. Experimental and theoretical investigations of Lantana camara oil diffusion from polyacrylonitrile membrane for pulsatile drug delivery system. *Mater Sci Eng C-Mat Biol Appl*. 2014;41:292–300.
43. Pan B, Zhang D, Li H, Wu M, Wang Z, Xing B. Increased adsorption of sulfamethoxazole on suspended carbon nanotubes by dissolved humic acid. *Environ Sci Technol*. 2013;47(14):7722–8.
44. Zhang L, Yang L, Zhang X, Li J, Fan L, Beck-Broichsitter M, et al. Sustained therapeutic efficacy of budesonide-loaded chitosan swellable microparticles after lung delivery: influence of in vitro release, treatment interval and dose. *J Control Release*. 2018;283:163–74.
45. Manna S, Donnell AM, Kaval N, Al-Rjoub MF, Augsburg JJ, Banerjee RK. Improved design and characterization of PLGA/PLA-coated chitosan based micro-implants for controlled release of hydrophilic drugs. *Int J Pharm*. 2018;547(1–2):122–32.
46. Ma B, Zhuang W, Liu G, Wang Y. A biomimetic and pH-sensitive polymeric micelle as carrier for paclitaxel delivery. *Regenerat Biomater*. 2018;5(1):15–24.
47. Maiti C, Parida S, Kayal S, Maiti S, Mandal M, Dhara D. Redox-responsive Core-cross-linked block copolymer micelles for overcoming multidrug resistance in Cancer cells. *ACS Appl Mater Interfaces*. 2018;10(6):5318–30.
48. Chen M, Zhang Y, Chen Z, Xie S, Luo X, Li X. Synergistic antitumor efficacy of redox and pH dually responsive micelleplexes for co-delivery of camptothecin and genes. *Acta Biomater*. 2017;49:444–55.
49. Teo JY, Chin W, Ke X, Gao S, Liu S, Cheng W, et al. pH and redox dual-responsive biodegradable polymeric micelles with high drug loading for effective anticancer drug delivery. *Nanomed-Nanotechnology Biology and Medicine*. 2017;13(2):431–42.
50. Yi X, Zhao D, Zhang Q, Xu J, Yuan G, Zhuo R, Li F. Preparation of multilocation reduction-sensitive core crosslinked folate-PEG-coated micelles for rapid release of doxorubicin and tariquidar to overcome drug resistance. *Nanotechnology*. 2017;28(8).
51. Zhang L, Xu J, Wen Q, Ni C. Preparation of xanthan gum nanogels and their pH/redox responsiveness in controlled release. *Journal of Applied Polymer Science*. 2019;136(36).
52. Zhang Y, Zhang L, Lin X, Ke L, Li B, Xu L, et al. Dual-responsive nanosystem for precise molecular subtyping and resistant reversal of EGFR targeted therapy. *Chem Eng J*. 2019;372:483–95.
53. Ruiz-Gomez MJ, Souviron A, Martinez-Morillo M, Gil L. P-glycoprotein, glutathione and glutathione S-transferase increase in a colon carcinoma cell line by colchicine. *J Physiol Biochem*. 2000;56(4):307–12.
54. Li Y, Lin J, Zhi X, Li P, Jiang X, Yuan J. Triple stimuli-responsive keratin nanoparticles as carriers for drug and potential nitric oxide release. *Mater Sci Eng C-Mater Biol Appl*. 2018;91:606–14.
55. Zheng L, Zhang X, Wang Y, Liu F, Peng J, Zhao X, et al. Fabrication of acidic pH-cleavable polymer for anticancer drug delivery using a dual functional monomer. *Biomacromolecules*. 2018;19(9):3874–82.
56. Chen K, Cai H, Zhang H, Zhu H, Gu Z, Gong Q, et al. Stimuli-responsive polymer-doxorubicin conjugate: Antitumor mechanism and potential as nano-prodrug. *Acta Biomater*. 2019;84:339–55.
57. Wang Y, Wu Y, Li K, Shen S, Liu Z, Wu D. Ultralong circulating lollipop-like nanoparticles assembled with gossypol, doxorubicin, and Polydopamine via π - π stacking for synergistic tumor therapy. *Adv Funct Mater*. 2019;29(1):1805582.
58. Zhao X, Jin Y, Li L, Xu L, Tang Z, Qi Y, et al. MicroRNA-128-3p aggravates doxorubicin-induced liver injury by promoting oxidative stress via targeting Sirtuin-1. *Pharmacol Res*. 2019;146:104276–6.
59. Li K, Liu W, Zhao Q, Wu C, Fan C, Lai H, et al. Combination of tanshinone IIA and doxorubicin possesses synergism and attenuation effects on doxorubicin in the treatment of breast cancer. *Phytother Res*. 2019;33(6):1658–69.